Paper ID: 401

Computational Modeling of Urine Flow in Pelvi-Ureteric Junction (PUJ) Obstruction Integrating Discrete Phase Model: A Non-invasive Approach for Diagnostic and Urodynamic Study

Md Abdullah Al Mamun[1], Umma Habiba[2], Dr. Jahid Ferdous[3], and Dr. Mohammad Habibur Rahman[4]

[1, 2, 3] Department of Biomedical Engineering, Bangladesh University of Engineering and Technology, Dhaka 1205, [4] National Institute of Kidney Disease & Urology (NIKDU), Dhaka 1207

E-mail: abdullah@bme.buet.ac.bd[1],ummehabiba1005@gmail.com[2], ferdousj@bme.buet.ac.bd[3], and mohammadhabiburrahman749@gmail.com[4]

Abstract

Pelvi-ureteric junction (PUJ) obstruction is a significant clinical condition that impedes urine flow from the renal pelvis to the ureter, leading to complications such as hydronephrosis and compromised renal function. Traditional diagnostic approaches are often invasive, posing risks and discomfort to patients. This study presents a novel, non-invasive computational model that simulates urine flow dynamics in the presence of PUJ obstruction, incorporating the Navier-Stokes equations and the Discrete Phase Model (DPM) to analyze urine flow and particle trajectories. The obstruction impedes urine flow, leading to increased retention and deposition of particles, thereby prolonging the half-time for particle washout. It also leads to increased DPM particle concentration in the pelvis and decreased concentration in the ureter below the obstruction due to particle accumulation and flow impediment. These outcomes offer valuable insights into the obstruction's severity, which are vital for precise diagnosis strategies.

Keywords: Pelvi-ureteric junction, Discrete Phase Model (DPM), Navier-Stokes equations.

1. Introduction

Ureteral Obstruction is a pathological condition characterized by the partial or complete blockage of urine flow from the kidneys to the bladder through the ureters [1]. It can lead to a cascade of pathophysiological effects such as hydronephrosis [2], Renal Dysfunction, Vesicoureteral Reflux (VUR), Chronic Kidney Disease (CKD), etc. Though mortality from ureteral obstruction is low with early treatment, it can severely affect quality of life and lead to serious complications ultimately leading to death if untreated. Ureteral obstructions commonly occur at the ureteropelvic junction, the crossing of the iliac vessels, and the ureterovesical junction. It can result from either congenital factors like UPJ and VUJ obstructions in children [3] or acquired factors such as kidney stones, tumors, and surgical trauma in adults [4]. Studies have shown that congenital UPJ obstruction occurs in approximately 1 in 1,500 live births, making it one of the most common causes of pediatric hydronephrosis [5, 6]. The primary consequence of PUJ obstruction is the impairment of urine drainage from the kidney which can lead to a buildup of urine in the renal pelvis, causing distention and increased pressure on the kidney.

The use of CFD in the study of ureteral obstruction represents a significant advancement in urology, offering a detailed and dynamic understanding of how obstructions impact urine flow. A study demonstrated a direct correlation between the obstruction severity and elevated pressure and shear stress leading to increased backflow within the ureter [7, 8]. Kidney stones originate in the kidney and often become lodged in the ureter, obstructing urine flow and causing severe pain [9, 10]. The effectiveness of DTPA renography in diagnosing PUJ obstruction was demonstrated by analyzing radiotracer time-activity curves and identifying significant obstructions through characteristic delayed excretion and altered curve patterns [11]. Vesicoureteral reflux (VUR) can contribute to urinary tract infections and stone formation [12]. While congenital anomalies at the ureteric-vesicular junction (UVJ) are commonly implicated in infants, increased intra-vesicular pressure during voiding can also predispose adults to VUR [13].

The diagnosis of ureteral obstruction involves a combination of medical history, physical examination,

and imaging studies such as ultrasound, CT-Urography, DTPA-Renography, and MRU. The severity of the obstruction and the function and drainage of the kidneys are evaluated by a DTPA renogram test that uses different radioactive agents. DTPA renogram results help to finally determine whether the doctor will go for surgery or not. Parameters such as the renal uptake rate, time to peak activity, and the time-activity curve slope are used to assess the degree of obstruction and its functional consequences. Studies have shown that these parameters can correlate with the degree of hydronephrosis and renal impairment, providing a quantitative measure of obstruction severity. The hallmark of PUJ obstruction on DTPA renogram is delayed or diminished clearance of the radiotracer from the obstructed kidney, which leads to accumulation of tracer in the renal pelvis and delayed excretion.

While existing diagnostic modalities provide valuable information, they are often limited in their ability to accurately quantify obstruction severity, and capture the dynamic nature of urine flow, pressure gradient, and urine retention. Additionally, current methods are often invasive, costly, and uncomfortable, with risks of radiation exposure and complications from contrast agents to the patients, especially for infants and pregnant women. The accuracy and interpretation of DTPA renogram results can be influenced by patient factors such as hydration status, bladder fullness, and patient cooperation during the procedure. Conversely, in medium and low-income countries like Bangladesh, diagnostic tests are available only in a limited number of designated locations. Additionally, there is a lack of sensitivity for early detection of partial or intermittent obstructions, potentially leading to delayed treatment and progressive renal damage. Therefore, it is crucial to investigate alternative approaches that effectively address these challenges while providing a non-invasive, dynamic assessment of obstruction severity and kidney function impact.

This study integrates computational fluid dynamics (CFD) with the Discrete Phase Model (DPM) to simulate the complex flow of urine and the movement of particles in the pelvic ureteric junction obstructed ureter. The developed computational model aims to provide insights into the hydrodynamics of the system, helping in the early diagnosis and characterization of PUJ obstructions and optimizing treatment strategies. Additionally, particle tracking simulations will be conducted to identify regions where urine retention may occur, mimicking the process of a DTPA renogram test.

2. Methodology

Computational domain and grid generation

Due to the scarcity of patient-specific CT scan data for Pelvi-Ureteric Junction (PUJ) obstructions, this study employed simplified 2D ureter models, incorporating varying degrees of PUJ obstruction ranging from mild to severe [Fig. 1]. The typical length of the male ureter ranges from 150 mm to 290 mm [14], with a diameter between 1.5 mm and 8 mm [15]. In this study, a ureter length of 280 mm was selected, with a fluid flow channel diameter ranging from 1.75 mm to 8 mm. The ureter has three natural constrictions (PUJ, VUJ, iliac artery bifurcation) where stones often get stuck [16]. Our modeled ureter narrowed at these points, with the PUJ being the narrowest (3.0 mm) and the VUJ being slightly wider (2.00 mm) than the iliac artery crossing (1.8 mm).

A comprehensive mesh convergence study was conducted utilizing the average velocity of urine to determine the optimal mesh resolution [Fig. 1(d)]. To refine the boundary layer, eight layers of inflation were applied with a growth rate of 1.2 and a maximum thickness of 0.4 mm [Fig. 1(c)]. The meshing process employed quadrilateral-dominant elements using a patch-independent algorithm. Mesh quality was assessed based on skewness and orthogonal quality, which measure the deviation of element shapes from ideal equilateral configurations.

Governing equations and numerical simulation

The urine flow in the human ureter model with particle tracers represents a two-phase flow, requiring separate solutions for the fluid and particle phases. The flow of urine is modeled using the Navier-Stokes equation for momentum and the continuity equation for mass. The continuity equation and the Navier-Stokes equation for an incompressible flow can be stated as follows:

$$\frac{\partial \rho}{\partial t} + \nabla \cdot (\rho v) = 0 \tag{1}$$

$$\rho\left(\frac{\partial v}{\partial t} + v \cdot \nabla v\right) = -\nabla p + \mu \nabla^2 v + \rho g \tag{2}$$

Here, ρ represents fluid density, v is the velocity vector, p denotes pressure, and μ signifies fluid viscosity. The discrete phase model (DPM) was applied to analyze tracer particle dynamics (PD) by solving the force

balance equation through the Euler-Lagrangian approach. The equation governing particle velocity in a Cartesian coordinate system is formulated as:

$$\frac{\partial u_p}{\partial t} = F_D(u - u_p) + \frac{g(\rho_p - \rho)}{\rho_p} \quad (3)$$

The term $F_D(u - u_p)$represents the drag force per unit mass of the particle. The discrete phase particle's trajectories are analyzed by integrating the force balance equation acting on each particle. The CFD simulations were performed utilizing the ANSYS Fluent 18.1 software package. The finite-volume method was employed to discretize the governing equations. To improve accuracy in predicting flow irregularities and instabilities, the k-epsilon realizable turbulence model was employed. Spatial discretization was carried out using the Green-Gauss Cell-based method. Convergence was achieved by ensuring that the relative fluctuation between consecutive iterations stayed below a pre-set threshold of 10^{-6}.

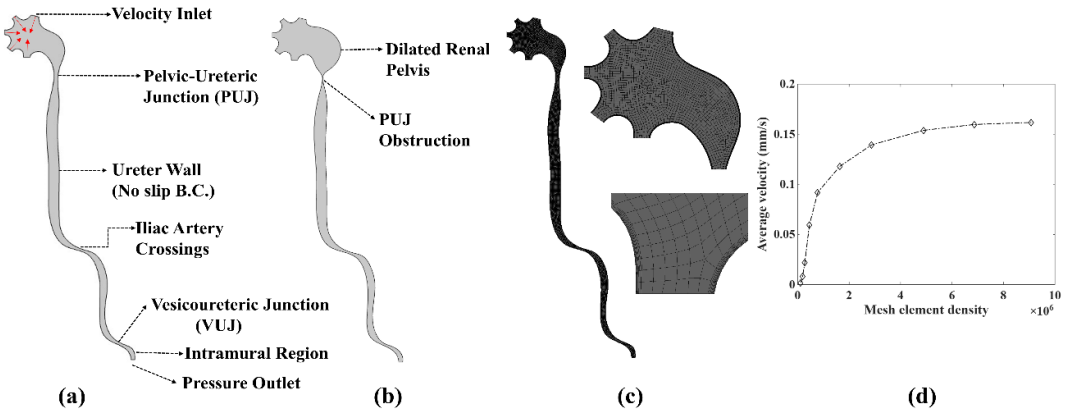


Fig. 1. Graphical Representation of 2D Ureter Models. (a) Three normal anatomical sites of constriction of the ureter (b) Introduction of ureteral strictures at the pelvic ureteric junction (c) Computational grid generation of 2D ureter models (d) Grid independence study

Material properties and boundary Conditions

The urine flow within the ureter was modeled as an incompressible fluid with a constant density of 1050 kg/m ^{3}and a viscosity of 1.3 cP [17]. Parabolic velocity profiles were employed as inlet boundary conditions, obtained from a pressure gradient of 0.3 Pa between the inlet and outlet, while a constant outlet pressure of 129.7 Pa was applied as the outlet boundary condition [18]. A no-slip boundary condition was enforced at the ureter walls.

In our investigation of the DPM renogram curve, the vascular phase of the DTPA renogram curve was deliberately excluded, as the vasculature was not incorporated into the model. To replicate the uptake phase of radioactive agents of the DTPA Renogram test, tracer particles were injected for a duration of up to 5 minutes. We utilized inert tracer particles with a uniform distribution. The Discrete Random Walk model was employed for stochastic particle tracking, while the Syamlal O'Brien drag law was applied to simulate particle-fluid interactions. As a result of the interaction with the surrounding continuous phase of urine flow, which propels them through the ureter, the velocity of tracer particles at the inlet was set to nearly zero (1e-6 m/s), perpendicular to the inlet edge.

3. Results and discussions

To elucidate the dynamics of ureteral fluid flow, we constructed two-dimensional ureteral models with varying different degrees of obstruction. By analyzing the velocity streamlines and spatial distribution of pressure gradients within these models, we have observed that the maximum urine velocity is significantly elevated as it traverses the three anatomical constriction regions of the ureter. However, the velocity subsequently diminishes, indicating a complex interplay between the ureteral geometry and fluid dynamics [Fig. 2(a)]. Furthermore, we have found that the pressure within the ureter undergoes a multi-step decrease following passage through the constrictions [Fig. 2(b)]. The deposition of tracer particles, as visualized in Fig. 2(c), is concentrated upstream of the obstruction, highlighting the obstruction's significant impact on particle transport within the ureter.

Fig. 3(a) shows that once the occlusion reaches 70%, the maximum wall shear stress (WSS) rises sharply, serving as an indicator of the severity of PUJ obstruction. The maximum velocity and turbulent

kinetic energy (TKE) of urine flow exhibit notable variations around the PUJ obstruction [Fig. 3(b), Fig. 3(d)]. Higher velocities and elevated TKE values are observed near the obstruction site, particularly in cases of severe narrowing, indicating increased flow disturbance and turbulence in the vicinity of the occlusion. The presence of a PUJ obstruction results in a significant pressure gradient across the ureter model [Fig. 3(c)]. As the obstruction becomes more severe, the pressure gradient increases, indicating a greater resistance to flow. This increased pressure can contribute to hydronephrosis, a condition characterized by the dilation of the renal pelvis due to the buildup of urine.

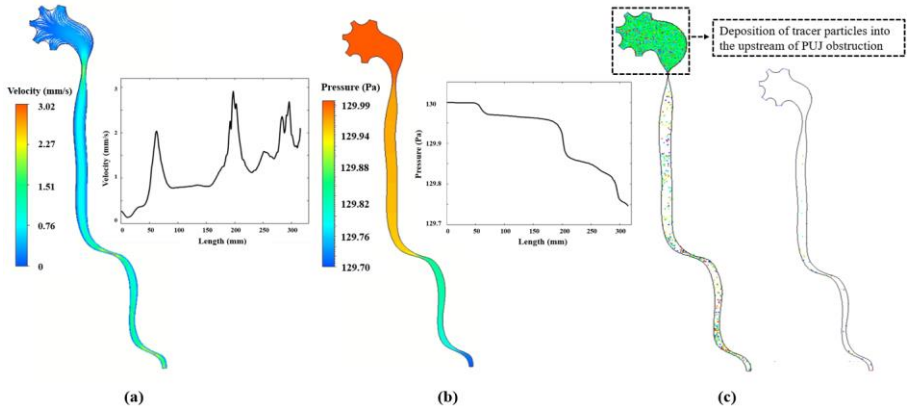


Fig. 2. Spatial distribution of velocity and pressure gradients in normal ureter models and tracer particle deposition in severely obstructed ureter at the upstream of pelvic-ureteric junction (PUJ)

The graphs depicted in Fig. 4(a) illustrate the impact of PUJ obstruction on tracer particle dynamics within ureter models. As the degree of occlusion increases, the rate of tracer particle discharge from the ureter models progressively decreases [Fig. 4(a), 4(b)]. These findings suggest that PUJ obstruction hinders the efficient movement of tracer particles through the ureter, leading to delayed clearance and potential accumulation of tracer particles. The normal ureter, with no occlusion, exhibited the most rapid discharge of tracer particles and the 50% occlusion curve shows a moderate discharge of tracer particles, while the 70% and 85% occlusion curves demonstrate significantly delayed discharge of tracer particles, reflecting the obstruction's impact on particle movement. In a normal ureter, the half-life and washout time of tracer particles are relatively short, reflecting efficient and rapid clearance. However, as the degree of obstruction increases, both the half-life and washout time of the tracer particles are extended [Fig. 4(c)].

The slope of the tracer particle washout DPM Renogram curve represents the rate at which tracer particles are cleared from the ureter. A steeper slope indicates a faster rate of clearance, while a shallower slope suggests a slower rate of clearance. The slope of the tracer particle washout DPM Renogram curve, as shown in Fig. 4(d), demonstrates a linear relationship between the degree of ureteral occlusion and the

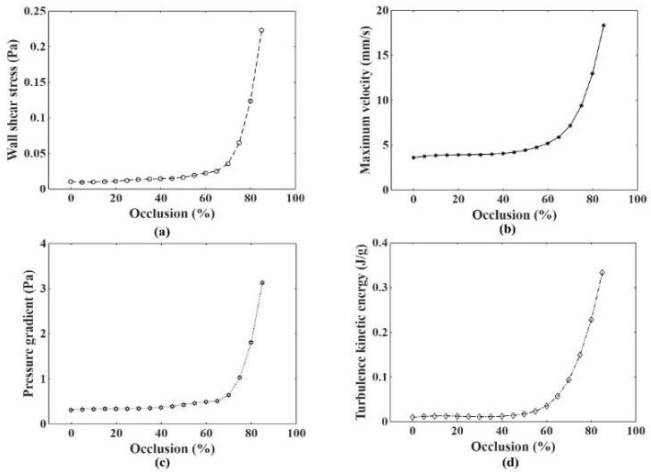


Fig. 3. Impact of PUJ Obstruction on different urodynamic parameters. (a) Variation of maximum wall shear stress on ureter wall (b) Maximum velocity in urine flow dynamics (c) Variation of pressure gradient across the ureter model (d) Variation of maximum turbulent kinetic energy in urine flow dynamics

rate at which tracer particles are cleared from the ureter. As the level of occlusion increases, the slope of the curve becomes steeper, indicating a slower rate of particle clearance.

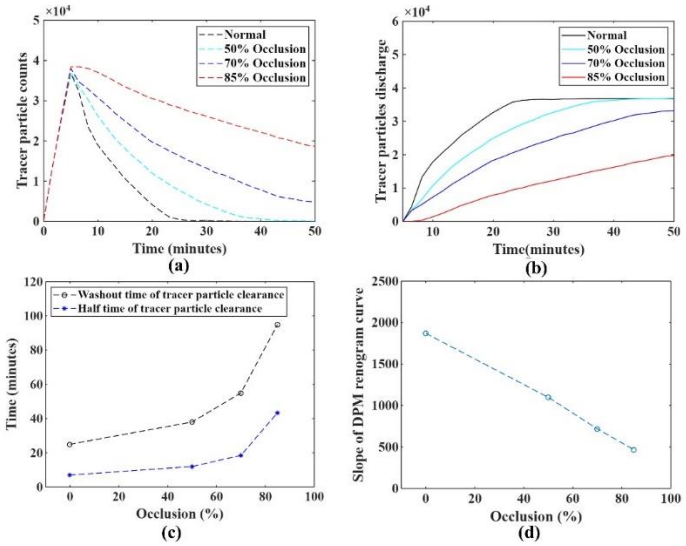


Fig. 4. Analyzing the impact of PUJ obstruction on tracer particle dynamics (a) DPM Renogram curves depicting the amount of tracked tracer particles (b) Discharge of tracer particles from ureter models through outlet (c) Half time and washout time of tracer particles (d) Slope of DPM Renogram curve during washout

The study depicts that the rate of decrease in particle concentration is significantly influenced by the severity of the obstruction. With higher levels of occlusion, the particle concentration decreases more slowly, indicating a reduced clearance efficiency [Fig. 5(a)]. This suggests that the obstruction impedes the movement of particles downstream, leading to their accumulation in the upstream region of PUJ obstruction. The normal condition shows the lowest peak particle concentration, while the 85% occlusion case has the highest, indicating a strong correlation between obstruction severity and particle accumulation. As the severity of the obstruction increases, urine flow becomes increasingly restricted, leading to increased retention in the renal pelvis. In contrast to the upstream region, the downstream particle concentration initially increases with time before reaching a plateau. This is likely due to the delayed arrival of particles that have been trapped in the upstream region. However, the plateau level is higher for higher levels of obstruction, indicating a greater accumulation of particles in the downstream region [Fig. 5(b)].

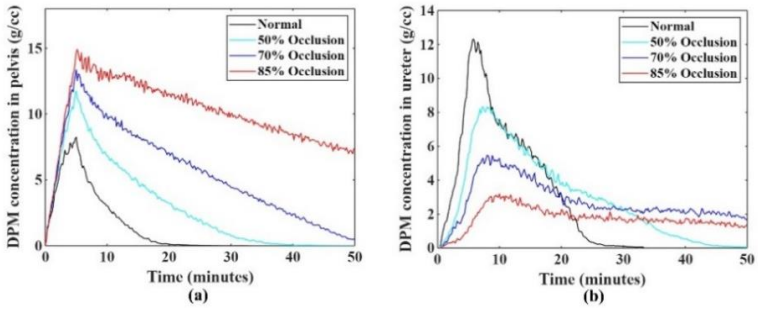


Fig. 5. Impact of PUJ Obstruction on tracer particle deposition. (a) Tracer particle concentration upstream of the PUJ obstruction (b) Tracer particle concentration downstream of the PUJ obstruction

Particle deposition within the ureter is closely linked to obstruction severity, flow velocity, and turbulence, providing valuable insights into areas of impaired clearance or stagnation indicative of compromised urine flow. Diagnostic methods like the DTPA renogram identify a renal clearance half-time of less than 10 minutes as normal, while values exceeding 15 minutes suggest significant upper urinary tract obstruction [19]. This scan reveals delayed clearance caused by the accumulation of radioactive particles upstream of the obstruction. Our findings demonstrate that a 70% luminal occlusion is sufficient to cause such clearance delays. Regions of increased particle retention align with higher obstruction severity, serving as reliable diagnostic markers for disrupted urodynamics.

4. Conclusions

This study introduces a novel computational model using the Discrete Phase Model (DPM) to simulate urine flow dynamics in PUJ obstruction, offering key insights into obstruction effects on urine clearance and particle distribution. Ureteral obstruction significantly affects tracer particle dynamics within the urinary tract, resulting in delayed clearance, reduced discharge, prolonged half-life, increased washout time, and decreased clearance rates, which underscore the serious consequences of the condition. Additionally, the model demonstrates a strong correlation between the severity of PUJ obstruction and urodynamic parameters, as well as particle deposition in the ureter. The study reveals that a 70% occlusion is enough to cause a substantial delay in clearance, surpassing the 15-minute threshold. This delay can serve as an early diagnostic indicator of obstruction, allowing for timely medical or surgical interventions to prevent complications like kidney damage or infection. By tracking the movement of tracer particles, clinicians can obtain valuable data on the severity and location of the obstruction, potentially aiding in the development of non-invasive diagnostic tools based on flow patterns and particle concentration. Moreover, particle deposition patterns offer insights into pressure and flow alterations upstream of the obstruction, aiding decisions between conservative treatments like hydration and invasive options such as stenting or surgical pyeloplasty. The study employs 2D ureter models to test the concepts of our hypothesis, as there is a limited availability of patient-specific CT scan data for PUJ obstructions. However, 2D ureter models cannot fully replicate the complex anatomy of the ureter and have limitations in capturing intricate flow dynamics, including vortices, flow separation, and backflow, which can slightly affect fluid flow patterns. As a result, future research could focus on developing complex 3D ureter models to achieve a more accurate representation, encompassing both PUJ and VUJ obstructions. Finally, by refining and expanding this computational model into a more realistic 3D simulation, researchers can contribute to the development of more effective and personalized approaches for the management of PUJ obstruction.

5. References

[1] Tanagho, E. A., & Pugh, R. C. B. (2001). Smith's general urology. McGraw-Hill Professional.

[2] Bajpai M, Bal CS, Tripathi M, Kalaivani M, Gupta AK. Prenatally diagnosed unilateral hydronephrosis: prognostic significance of plasma renin activity. J. Urol. 2007; 178; 2580–2584.

[3] R.M. Morse, M.I. Resnick, Ureteral calculi: natural history and treatment in an era of advanced Technology, J. Urol. 145 (2) (Feb. 1991) 263–265.

[4] Glassberg, K. I., et al. (2015). Ureteropelvic Junction Obstruction: Pathogenesis and Clinical Features. Journal of Urology, 193(4), 1013-1020.

[5] Resnick, M. I., & Sutherland, D. J. R. (2004). Urology: clinical practice and research. Elsevier.

[6] Beetz, R. (2008). Evaluation and management of congenital anomalies of the kidney and urinary tract. Current Opinion in Pediatrics, 20(2), 163-168.

[7] Senguttuvan, P. and Jigy, J., 2014. Profile and outcome of pelvic ureteric junction obstruction. The Open Urology & Nephrology Journal, 7(1).

[8] R.J. Lang, M.A. Tonta, B.Z. Zoltkowski, W.F. Meeker, I. Wendt, H.C. Parkington, Pyeloureteric peristalsis: role of atypical smooth muscle cells and interstitial cells of Cajal-like cells as pacemakers, J. Physiol. 576 (3) (Nov. 2006) 695–705.

[9] D.J. Griffiths, Flow of urine through the ureter: a collapsible, muscular tube undergoing peristalsis, J. Biomech. Eng. 111 (3) (Aug. 1989) 206–211.

[10] C.Y. Pak, J.R. Poindexter, B. Adams-Huet, M.S. Pearle, Predictive value of kidney stone composition in the detection of metabolic abnormalities, Am. J. Med. 115 (1) (Jul. 2003) 26–32.

[11] R.L. Drake, W. Vogl, A.W.M. Mitchell, Gray's Anatomy for Students, Elsevier, 2019.

[12] Arant, B. S., 1991. “Vesicoureteric reflux and renal injury. American journal of kidney diseases, 17(5), pp. 491–511.

[13] Iannaccone, G., and Panzironi, P. E., 1955. “Ureteral reflux in normal infants”. Acta radiologica, 44(6), pp. 451–456.

[14] Majd, M., Bar-Sever, Z., Santos, A.I. and De Palma, D., 2018. The SNMMI and EANM procedural guidelines for diuresis renography in infants and children. Journal of Nuclear Medicine, 59(10), pp.1636-1640.

[15] Kohler, Tobias, Mitchell Yadven, Ankur Manvar, Nathan Liu, and Manoj Monga. "The length of the male urethra." International braz j urol 34 (2008): 451-456.

[16] Itanyi, Ukamaka Dorothy, et al. "Assessment of ureteric diameter using contrast-enhanced helical abdominal computed tomography." African Journal of Urology 26 (2020): 1-5.

[17] Vahidi, Bahman, Nasser Fatouraee, Ali Imanparast, and Abbas Nasiraei Moghadam. "A mathematical simulation of the ureter: effects of the model parameters on ureteral pressure/flow relations." (2011): 031004.

[18] Razavi, Seyed Esmail, and Mohammad Jouybar. "Simulation of urine flow in a ureter with vesicoureteral reflux and primary obstructed megaureter by fluid–structure interaction." Biomed Mater Eng 1 (2018): 1-17.

[19] Taylor, Andrew T et al. “SNMMI Procedure Standard/EANM Practice Guideline for Diuretic Renal Scintigraphy in Adults With Suspected Upper Urinary Tract Obstruction 1.0.” Seminars in nuclear medicine vol. 48,4 (2018): 377-390.